Universität Karlsruhe (TH)
Institut für Baustatik

Systematic Prediction of Yield-Line Configurations for Arbitrary Polygonal Plates

J. Wüst, W. Wagner

Mitteilung 2(2007)

Universität Karlsruhe (TH)
Institut für Baustatik

Systematic Prediction of Yield-Line Configurations for Arbitrary Polygonal Plates

J. Wüst, W. Wagner

Mitteilung 2(2007)

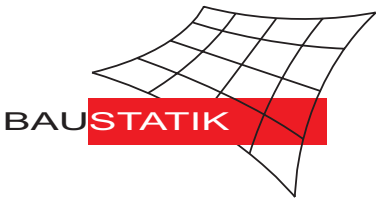

Prof. Dr.–Ing. W. Wagner
Institut für Baustatik
Universität Karlsruhe
Postfach 6980
76128 Karlsruhe

Telefon: (0721) 608–2280
Telefax: (0721) 608–6015
E–mail: bs@.uni-karlsruhe.de
Internet: http://www.bs.uni-karlsruhe.de

Systematic Prediction of Yield-Line Configurations for Arbitrary Polygonal Plates

J. Wüst
Ingenieurgruppe Bauen,

Hübschstraße 21
D-76135 Karlsruhe
Germany

W. Wagner
Institut für Baustatik
Universität Karlsruhe (TH)
Kaiserstraße 12
76131 Karlsruhe
Germany

Contents

Abstract

In addition to the well established finite element method in recent years several optimization approaches have been developed concerning the yield-line theory. This paper presents a new systematical algorithm to predict initial yield-line configurations of arbitrary polygonal plates. It contributes a solution to the task of detecting yield-line patterns in advance of an optimization process. For this reason a ciphering of yield-line patterns is proposed and a new application of Catalan numbers and binary trees is demonstrated. After a subsequent refining a triangular element is used in combination to a simplex optimization procedure in order to determine the ultimate load of the considered yield-line configuration. Moreover, further optimization strategies like the direct search method and the conjugate gradient method lead to the final solution of the problem. The use and the efficiency of the new approach are demonstrated with three examples.

1 Introduction

The yield-line theory is employed to achieve a fast calculation of the ultimate load of plates. Laminar zones of plasticity are concentrated in yield lines which border rigid parts of the plate. Thus a kinematical admissible failure mechanism is provided and the ultimate load can be determined based on the energy theorem.

In the historical retrospect, the yield-line theory is mainly based on the work of [9] who shaped the method decisively in the middle of the 20th century. But the increasing spread of computers advantaged more and more the development of other or refined methods. However, some important impulses have been presented by [1] and especially by [15]. They proposed a triangular element mapping all possible interactions between edge rotations and nodal displacements, see Section 4. With its aid, the kinematic parameters are represented and based on the simplex optimization method. The ultimate load of a correctly triangulated plate is found whereas the nodal coordinates are considered to be immovable.

In recent years, research focused on the improvement of the predetermined yield-line pattern. For this reason an extended application of optimization strategies is obvious. [17] presented an approach starting with a regularly triangulated plate structure out of which the active yield-lines are discovered. The final yield-line pattern is detected by a direct search procedure. In contrast to that, [13] and [19] used a specially adapted gradient method to optimize a comparatively coarse triangular mesh. Both optimization procedures will be analyzed in context to the presented approach of an automatically detected yield-line pattern.

2 Basic considerations

2.1 Concept of the yield-line theory

First of all the general properties of the yield-line theory are introduced. The concept is based on the upper bound of the ultimate load. This load is calculated using the virtual displacements of a kinematical system formed by yield-lines. The procedure corresponds to the method of plastic hinges for rods and beams. Amongst other aspects there are some general assumptions concerning the material behaviour. Plastic zones of the deformed slab

are transformed to yield-lines enclosing rigid planes. The yield condition is considered to be elastic ideally-plastic. Once reached the ultimate bending moment remains constant without any hardening. This leads to the assumption that both the plastic bending moment and the ability to rotate are constant along a yield-line as well. There are no changes concerning the thickness of the slab and the distribution of stresses in the cross section is also idealized. In this way the material properties are entirely expressed within a positive and a negative plastic moment acting on the lower and upper side of the plate respectively.

2.2 Principle of virtual displacements

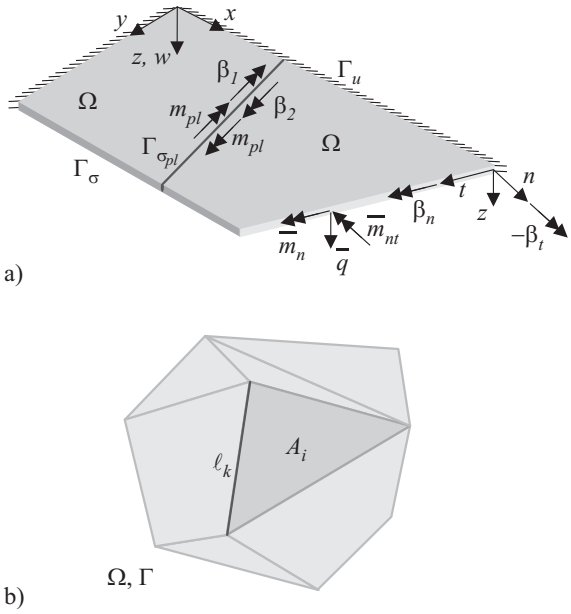

Figure 1: a) Plate domain Ω with boundaries Γ and b) Rigid plane surrounded by yield-lines Γ

Using Galerkin's method, equilibrium has to be fulfilled with $\delta\Pi = 0$. Assuming that the interior work is concentrated at yield-lines a partial integration over the integration area Ω and along the boundaries Γ formed by yield-lines leads to

$$-\int_{\Gamma_{\sigma_{pl}}} \delta\theta \; m_{pl} \; ds \; + \int_{\Omega} \delta w \; p \; dA \; + \int_{\Gamma_\sigma} \delta \boldsymbol{u}^T \; \bar{\boldsymbol{t}} \; ds \; = \; 0 \; , \tag{1}$$

with the angle $\delta\theta = \delta\beta_2 - \delta\beta_1$, see Fig. 1a. Since yield-lines are considered to be straight and external work performed by constant area loads act upon several rigid planes, see Fig. 1b, the fundamental equation is given for n_k yield-lines and n_i rigid plates by

$$\sum_{k=1}^{n_k} (m_{pl,k} \; \ell_k \; \delta\theta_k) = \sum_{i=1}^{n_i} \int_{A_i} p \; \delta w \; dA_i \; , \tag{2}$$

where $m_{pl,k}$ signifies the plastic moment of the yield-line and δw is the displacement perpendicular to the plate caused by the area load p while external loads at the boundaries Γ_σ are neglected for simplicity.

2.3 Geometrical considerations

As a result of the claim for kinematical admissibility yield-lines have to be linear without any break. Each supported edge of the slab forms the rotating axis of a rigid plane which is bordered by yield-lines. So the number of rigid planes corresponds to the number of supported edges. The yield-line between two rigid planes arises from the point of intersection of the associated rotating axes. This rule applies to not adjoining edges accordingly whereas parallel axes produce parallel yield-lines. Within the slab three or more yield-lines come across each other in so-called branching points. Together they generate a yield-line pattern which leads to a kinematical admissible collapse mechanism. In view of these geometric facts an obvious way to generate yield-line patterns is to rotate rigid planes around their rotation axes as it is proposed by [12]. The intersection of three planes yield the corresponding branching point. This comprehensible approach permits also the consideration of free edges by rotating the according plane perpendicular to its initial position, see Fig. 2. In this way a possibility to detect the coordinates of branching points is given. But since there are several possibilities of intersection modes it is important to introduce a system to describe branching points and yield-lines. This demand is underlined by the experience that even if the angles of the rotation axes are defined the resulting yield-line pattern will not be necessarily unique; in this context see also [7].

2.4 Description of yield-line patterns

Due to the fact that supported edges are in general related directly to the adjacent rigid plane, the number of both is equal. The yield-line bordering two adjoining rigid planes is defined by their two numbers. Thus all yield-lines which enclose a rigid plane get its number as Fig. 3 illustrates. Points of intersection of yield-lines are at the same time a connection between three or more rigid planes. In the special case of an intersection of more than three yield-lines which means a conjunction of at least four rigid planes, this point of intersection will be divided into several branching points with the same coordinates. Thus one branching point always marks the connection between three yield-lines. Since two adjoining yield-lines bear one common number, the branching point is exactly defined by three different numbers. Two branching points connected by a yield-line possess the two ciphers of which. Furthermore, the existence of branching points owning the same two ciphers more than twice is impossible

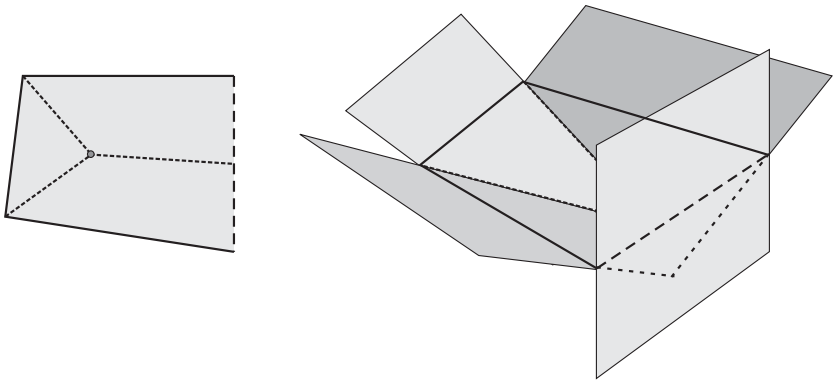

Figure 2: Intersection of rotated planes

as well as the multiple appearance of one and the same cipher within the three-digit code. In the case of an intersection of four yield-lines and more there exists more than one possibility to encode as it is shown in Fig. 4.

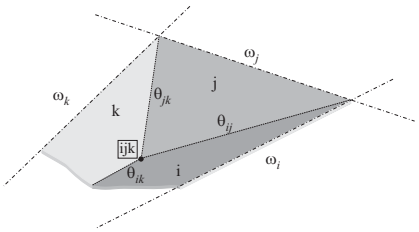

Figure 3: Ciphering of branching point

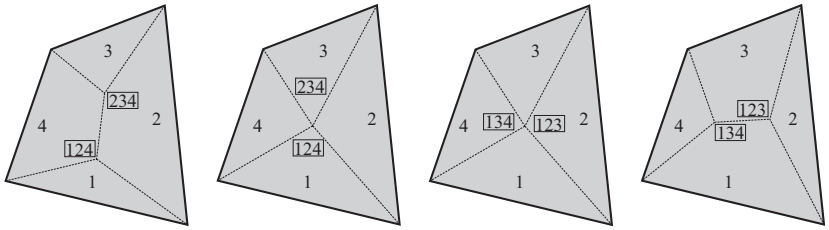

Figure 4: Ciphering of multiple intersection of yield-lines

3 Algorithm for yield-line prediction

3.1 Theoretical aspects

The preceding pictures of yield-line patterns illustrate that the number of branching points depends on the number of rigid planes. Three fractions of the plate have one common branching point and every further fraction part causes one more point. Thus, e.g. a pentagonal plate possesses three branching points. For an arbitrary polygonal plate the number of branching points can be calculated with the relation

$$p = n - 2 \tag{3}$$

where p is the number of branching points and n the number of edges.

For the prediction of yield-line patterns it is necessary to know the amount of combinational possibilities. Their quantity k is linked with the number of supported edges. The number of a rigid plane cannot be used twice in the triple-digit ciphering of a branching point. Thus we get the condition

$$k = \binom{n}{3} = \frac{n!}{3!\,(n-3)!} \tag{4}$$

which describes all possible combinations of numbers whereas permutations of the three digits are not permitted.

However, the number of real admissible yield-line configurations is considerably less. A yield-line always connects two branching points. Therefore the sequence of two numbers

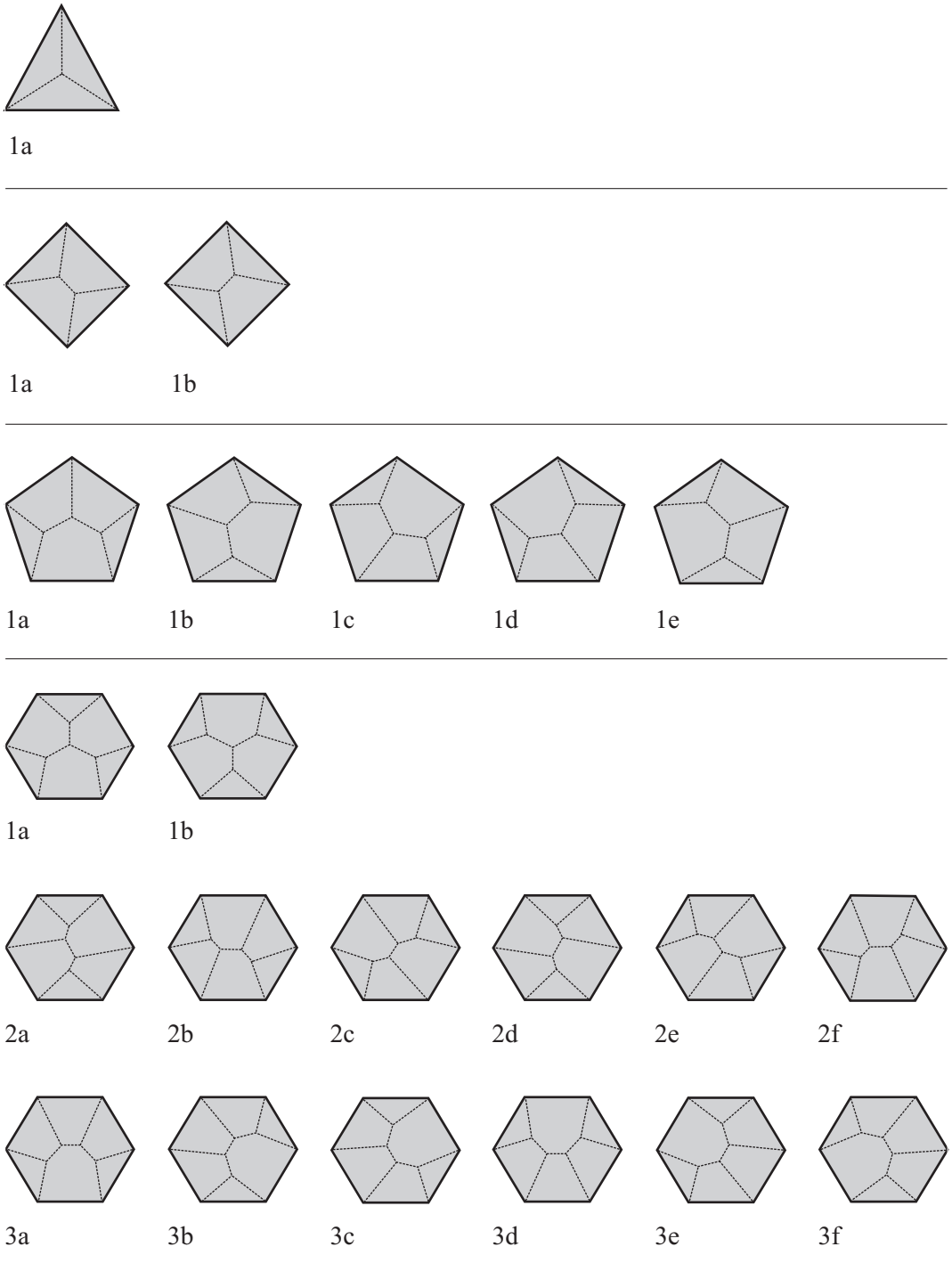

Figure 5: Examples of combinations and groups of configurations

may only appear twice in the digit combinations. This leads to a further reduction of the admissible combinations. The final amount of combinations $C_n(p)$ related to the number of edges n and branching points p is given in Table 1.

Table 1: The number of admissible branching point combinations

n	3	4	5	6	7	8	9	10
p	1	2	3	4	5	6	7	8
$C_n(p)$	1	2	5	14	42	132	429	1430
N	1	1	1	3	4	12	27	82

The calculation rule of the sequence can be defined as

$$C_n\left(p\right) = \frac{1}{p+1}\binom{2p}{p} = \frac{(2p)!}{p\,!\,(p+1)!} \tag{5}$$

and the obtained sequence is known as the Catalan numbers, see [3].

Amongst others, Fig. 5 demonstrates the combinations of yield-line patterns of a hexagonal plate. Some patterns simply are a permutation of the same configuration whereas the hexagon is the first polygon to find several different configurations. The fourteen combinations can be divided into three different groups of yield-line configurations.

The number of different configurations can be computed depending on the according Catalan number, see [18],

$$N = \frac{1}{2\,(p+2)}\,C_n\left(p\right) + \frac{1}{3}\,C_n\left(\frac{p-1}{3}\right) + \frac{3}{4}\,C_n\left(\frac{p}{2}\right) + \frac{1}{2}\,C_n\left(\frac{p-1}{2}\right)\,. \tag{6}$$

3.2 Computational code of the configurations

Fig. 6 illustrates that the run of a yield-line pattern can be considered as a binary tree. As mentioned in the preceding section, the yield-line combinations of a pentagonal plate are the permutation of one single configuration. If we choose each angle of the pentagon as the root of a binary tree, we get five different runs.

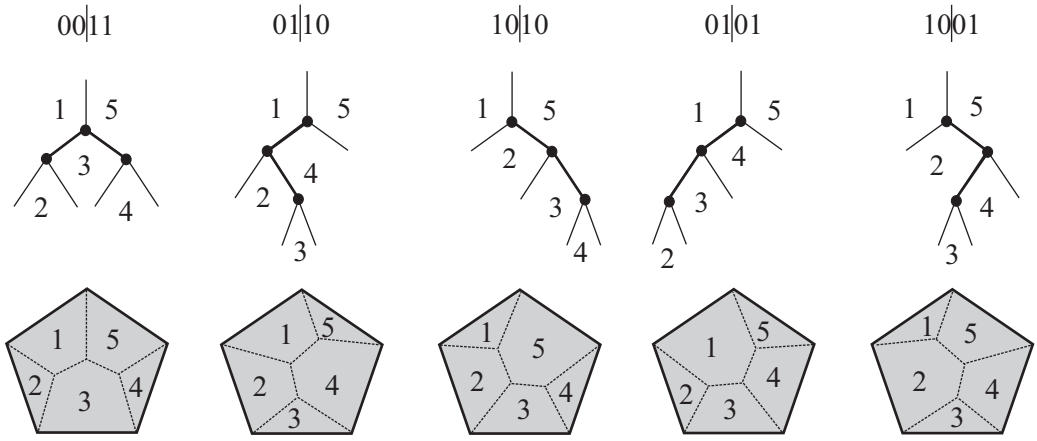

Figure 6: Binary code and binary tree of yield-lines

Table 2: Assembly instructions

Sequence	00	01	10	11
a	$a_i \rightarrow a_{i+1}$	$a_i \rightarrow a_{i+1}$	$*$	$*$
b	$b_i \rightarrow c_{i+1};\ S_1$	$b_i \rightarrow c_{i+1}$	$b_i \rightarrow a_{i+1}$	$S_1 \rightarrow a_{i+1}$
c	$c_i \rightarrow S_2$	$*$	$c_i \rightarrow c_{i+1}$	$S_2 \rightarrow c_{i+1}$

$*$ = backward calculation at a break or end of a branch

[2] present a system to describe problems related to Catalan numbers. They introduce a method to compile binary code sequences and to decode into binary trees. In the following this procedure is adapted to the requirements of the encoding of yield-line patterns, see [20]. Based on the code sequences the developed computer program composes a yield-line pattern according to the assembly instructions in Table 2. The sequence will be divided into blocks of two digits which describe the behaviour of yield-line branches in the branching points. According to the code instructions the digits of the triple-digit ciphering abc will be kept or changed. At the beginning we set $a_0 = 1$ and $c_0 = n$; b_0 is unknown. The stack $(S1; S2)$ management is "last in – first out".

The missing digits being marked with an asterisk are determined by a backward calculation which will be done at a break or at the end of a branch. The latter is specified by the fact that the three digits identifying a branching point have to be consecutive. A break signifies that two of them have to be consecutive, since two of the rigid planes forming the branching point are adjacent.

3.3 Binary Encoding

Another kind of application of Catalan numbers is the task to run through a quadratic grid from left top to right down without passing the diagonal. The path may only point to the right and downward direction as it can be seen in Fig. 7 with a 3×3 grid.

The numerical description is performed by a binary code noting the horizontal and vertical steps with 0 and 1, respectively. In this way all admissible binary codes are reproduced depending on the extension of the considered problem. Sequences have to include the same number of both ciphers. Since the first and the last step are fix, the first and the last cipher must also be unchangeable.

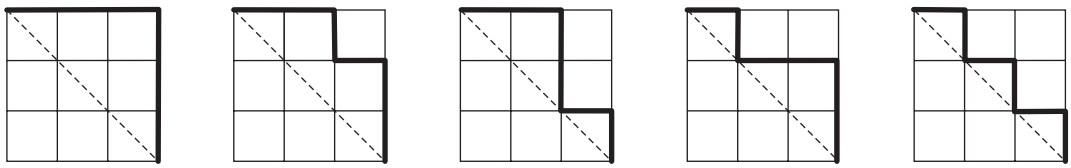

000111 001011 001101 010011 010101

Figure 7: Binary encoding grid

3.4 Example for the yield-line decoding

In the next step all admissible yield-line configurations are reproduced. With the binary code of 0010011110 the approach is illustrated. According to the length of ten ciphers it is clear that there are six branching points describing one of 132 yield-line patterns of an octagonal plate. So the initial situation is given by

$$a_0 = 1; \qquad b_0 = x_1; \qquad c_0 = 8\ .$$

The first two digits provide that the ciphering of the first branching point conserves the number of the first plate – see Table 2. However, the second one is put on the future third Figure and is stacked together with the contemporary one. Since a branch to the right is added corresponding to the next pair of ciphers which means the existence of two adjacent planes, the ciphering of the second branching point has to map this fact by using two adjacent numbers. According to the third block another branch to the left has to be adjoined. But in contrast to the first sequence the numbers will not be stacked. As the next pair of ciphers calls the stacked numbers and adds a right branch to the root, the present string ends. In consequence the fourth branching point possesses three consecutive numbers and the variable $x_2 = 4$ is detected. The new branch rising from the root to the right must contain the number of plane 8 as its third cipher. Afterwards it will be extended again to the right side. With the end of the binary code the remaining variables are detected as $x_4 = 7$ and $x_3 = 6$. Finally the last unknown is recovered with $x_1 = 5$.

In the following the steps are shown in detail:

Start:	$a_0 = 1;$	$b_0 = x_1;$	$c_0 = 8$				
00:	$a_1 = 1;$	$b_1 = 2;$	$c_1 = x_1;$	$x_1 \rightarrow$ S1;	$8 \rightarrow$ S2		
10:	$a_2 = 2;$	$b_2 = x_2;$	$c_2 = x_1$				
01:	$a_3 = 2;$	$b_3 = 3;$	$c_3 = x_2;$	$x_2 = 4$			
11:	$a_4 = x_1;$	$b_4 = x_3;$	$c_4 = 8;$	$x_1 \leftarrow$ S1;	$8 \leftarrow$ S2		
10:	$a_5 = x_3;$	$b_5 = x_4;$	$c_5 = 8;$	$x_4 = 7;$	$x_3 = 6;$	$x_1 = 5$	

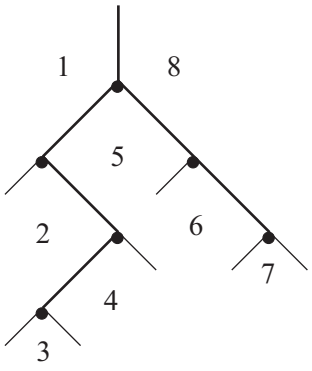

3.5 Consideration of the individual geometry

The individual geometry of the considered plate has not been discussed yet. The preceding step yields the theoretical admitted branching point combinations and their triple-digit ci-

phering. With this knowledge at hand the according coordinates are obtained by intersecting the corresponding three rigid planes. The latter will be rotated equally in their rotation axes. Thus we get a yield-line pattern based on the bisecting lines of the plate angles. In the next step the kinematical contradictions of the results are analyzed. Yield-lines may not cross each other and the coordinates of branching points have to be located within the plate. Furthermore the sum of the rigid plane areas has to be equal to the area of the entire plate. Finally the admissible yield-line patterns remain as a first prediction for the following yield-line calculation.

3.6 Triangulation

Up to now the structure only provides that the required yield-lines are represented within the plate topology. For the continuative calculation performed by the use of standardized plane elements it is necessary to create triangular segments being the simplest type of a plane. The triangles are produced by connecting the nodes of the plane polygons correspondingly to Fig. 8. In this way no additional nodes are created and the calculating effort is not increased. The course of the accessory yield-line is not significant because though it is decisive for the calculation matrix it does not affect the result of the ultimate load. In consequence the calculation reveals that the inserted yield-lines have no rotation angles and the adjacent planes act as one.

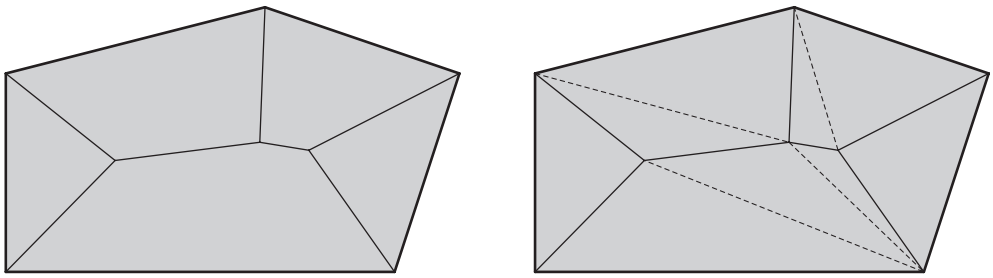

Figure 8: Triangulation of a pentagonal plate

4 Triangular element

After the determination of a yield-line pattern and its subsequent triangulation a plate element is employed, see [1] and [15]. Fig. 9 illustrates the relations between nodal displacements and edge rotations along yield-lines given by

$$\begin{bmatrix} \delta\theta_1^e \\ \delta\theta_2^e \\ \delta\theta_3^e \end{bmatrix} = \begin{bmatrix} -\dfrac{1}{h_1} & \dfrac{b_1}{\ell_1 h_1} & \dfrac{a_1}{\ell_1 h_1} \\ \dfrac{a_2}{\ell_2 h_2} & -\dfrac{1}{h_2} & \dfrac{b_2}{\ell_2 h_2} \\ \dfrac{b_3}{\ell_3 h_3} & \dfrac{a_3}{\ell_3 h_3} & -\dfrac{1}{h_3} \end{bmatrix} \begin{bmatrix} \delta w_1 \\ \delta w_2 \\ \delta w_3 \end{bmatrix} \tag{7}$$

or

$$\delta\boldsymbol{\theta}^e = \boldsymbol{E}^e \delta\boldsymbol{w}^e \ . \tag{8}$$

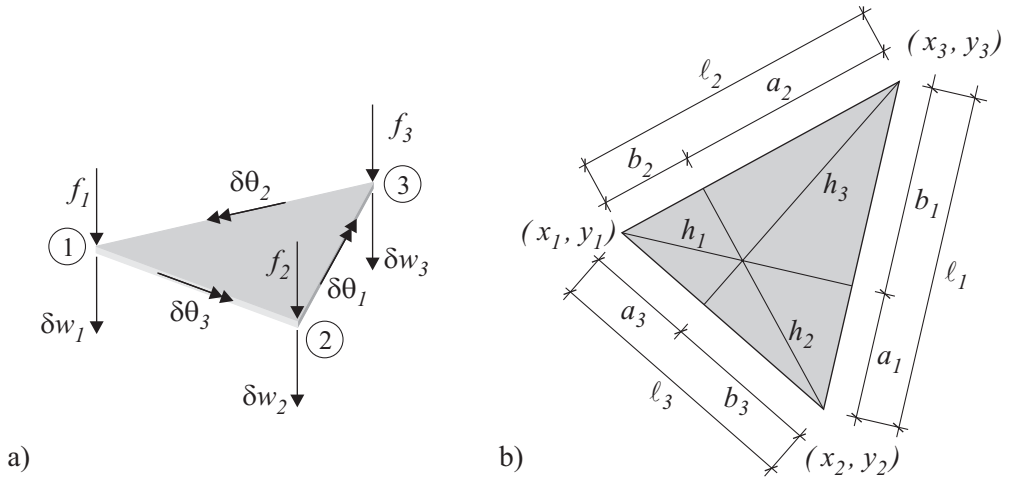

Figure 9: Triangular area element

Furthermore the element load vector for the distributed constant load p is defined with

$$\boldsymbol{f}^e = \begin{bmatrix} \frac{p\, h_1\, \ell_1}{6} \\ \frac{p\, h_2\, \ell_2}{6} \\ \frac{p\, h_3\, \ell_3}{6} \end{bmatrix} \tag{9}$$

which corresponds in a similar way to the vector $\boldsymbol{m}^e$ containing the plastic moments of the yield-lines with

$$\boldsymbol{f}^e = \boldsymbol{E}^{eT} \boldsymbol{m}^e \ , \tag{10}$$

see [14] and [16].

Using the identity matrix $\boldsymbol{I}$ the plastic moment vector $\boldsymbol{m}$ is divided into its positive and negative components,

$$\begin{bmatrix} \boldsymbol{I} \\ -\boldsymbol{I} \end{bmatrix} \boldsymbol{m} \leq \begin{bmatrix} \boldsymbol{m}_{pl}^{+} \\ \boldsymbol{m}_{pl}^{-} \end{bmatrix} \tag{11}$$

and the same principle applies to the rotation vector $\delta\boldsymbol{\theta}$ with

$$\delta\boldsymbol{\theta} = \begin{bmatrix} \boldsymbol{I} & -\boldsymbol{I} \end{bmatrix} \begin{bmatrix} \delta\boldsymbol{\theta}^{+} \\ \delta\boldsymbol{\theta}^{-} \end{bmatrix} . \tag{12}$$

Since positive yield-lines cause an extension of the lower side of the plate, $\boldsymbol{m}_{pl}^{+}$ is replaced by $\boldsymbol{m}_{pl,l}^{T}$. Similarly $\boldsymbol{m}_{pl,u}^{T}$ represents $\boldsymbol{m}_{pl}^{-}$ and finally the objective function reads

$$\begin{bmatrix} \boldsymbol{m}_{pl,l}^{T} & \boldsymbol{m}_{pl,u}^{T} \end{bmatrix} \begin{bmatrix} \delta\boldsymbol{\theta}^{+} \\ \delta\boldsymbol{\theta}^{-} \end{bmatrix} \rightarrow \min \ . \tag{13}$$

The kinematic relations are composed over the whole plate, following

$$\boldsymbol{E} = \bigcup_{e=1}^{numel} \boldsymbol{E}^e \ . \tag{14}$$

In the same manner the virtual displacements $\delta \boldsymbol{w}^e$ and the load vector $\boldsymbol{f}^e$ are summarized over the number of triangular elements. Together they define the scaled external work

$$\boldsymbol{f}^T \delta \boldsymbol{w} = 1 \ . \tag{15}$$

Equation (8) yields the constraints

$$\delta \boldsymbol{\theta}^+ - \boldsymbol{E} \delta \boldsymbol{w}^+ = \boldsymbol{0} \tag{16}$$
$$-\delta \boldsymbol{\theta}^- + \boldsymbol{E} \delta \boldsymbol{w}^- = \boldsymbol{0} \tag{17}$$

of the optimization.

By computing the optimization tableau

$$\boldsymbol{A} = \begin{bmatrix} \boldsymbol{0} & \boldsymbol{0} & \boldsymbol{f}^T & -\boldsymbol{f}^T \\ \boldsymbol{I} & -\boldsymbol{I} & -\boldsymbol{E} & \boldsymbol{E} \end{bmatrix} \ , \tag{18}$$

the right hand side

$$\boldsymbol{b} = \begin{bmatrix} 1 \\ \boldsymbol{0} \end{bmatrix} \tag{19}$$

and the plastic moment vector

$$\boldsymbol{c}^T = \begin{bmatrix} \boldsymbol{m}_{pl,l}^T & \boldsymbol{m}_{pl,u}^T & \boldsymbol{0} & \boldsymbol{0} \end{bmatrix} \tag{20}$$

the objective function and the constraints of an optimization approach are given,

$$\boldsymbol{c}^T \boldsymbol{x} \ \rightarrow \ \min \tag{21}$$
$$\boldsymbol{A} \boldsymbol{x} \ = \ \boldsymbol{b} \tag{22}$$
$$\boldsymbol{x} \ \geq \ \boldsymbol{0} \ . \tag{23}$$

Finally the vector $\boldsymbol{x}$ containing the virtual displacements and rotations $\delta \boldsymbol{w}$, $\delta \boldsymbol{\theta}$ is determined by performing a simplex optimization process.

5 Optimization strategies

After the calculation of the present yield-line pattern the result of the obtained ultimate load may be reduced by improving the position of the branching points. For this task there are in general two optimization procedures available. Both depend on the choice of an adequate yield-line pattern which was up to now left to the user.

5.1 Direct search method

A first possibility is to apply an approach proposed in [17] and is based on the direct search method by [6]. On the assembly of the optimization tableau $\boldsymbol{A}$ geometric constraints had to be set for the vertical displacements of the plate. The degrees of freedom $\boldsymbol{\chi}$ of the direct search method will be set in the same manner. Corner nodes as well as branching points being set upon a vertical point support will not move during the optimization process. Thus there remain only the branching points being able to improve the yield-line pattern structure

by moving, which may lead to a further reduction of the ultimate load towards a minimum. If it is necessary the coordinates are transformed into the considered direction, e.g. in the case when branching points have to move along free edges, see Fig. 10.

During the search trial steps are made into forward and backward search directions whereas the change of the calculation solutions is checked. In this way a successively improved yield-line pattern is achieved reducing the ultimate load result step by step. The procedure ends when no further reduction is found.

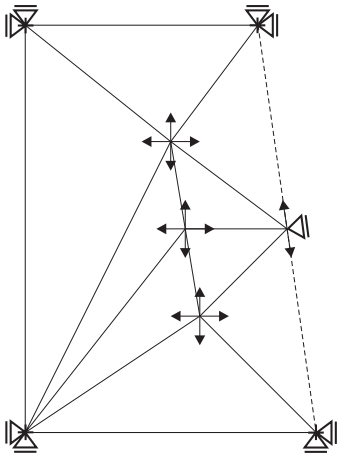

Figure 10: Search directions in a triangulated plate with a free edge

5.2 Conjugate gradient method

Another alternative is the application of the gradient search method by [5] which was employed in conjunction with the yield-line theory by e.g. [8], [13] and [19]. In order to determine the gradient vector $\boldsymbol{g}$ of the search direction the geometrical parameters ℓ, a, b and h shown in Fig. 9 have to be differentiated. The same holds for the components of the load vector $\boldsymbol{f}^e$. The number of the searching degrees of freedom $\boldsymbol{\chi}$ rules the dimension of the gradient vector,

$$\boldsymbol{g}\left(\boldsymbol{\chi}\right) \equiv \frac{\partial Z\left(\boldsymbol{\chi}\right)}{\partial \boldsymbol{\chi}} \ . \tag{24}$$

With the split of the optimization tableau $\boldsymbol{A}$ into $\boldsymbol{A}_B$ and $\boldsymbol{A}_N$ depending on the basic variables $\boldsymbol{x}_B$ and the non-basic variables $\boldsymbol{x}_N$ and a corresponding arrangement of the vector $\boldsymbol{c}$ follows

$$Z\left(\boldsymbol{\chi}\right) \ = \ \boldsymbol{c}_B\boldsymbol{x}_B + \boldsymbol{c}_N\boldsymbol{x}_N \tag{25}$$

$$\begin{bmatrix}\boldsymbol{A}_B & \boldsymbol{A}_N\end{bmatrix}\begin{bmatrix}\boldsymbol{x}_B \\ \boldsymbol{x}_N\end{bmatrix} \ = \ \boldsymbol{b} \tag{26}$$

$$\text{where} \quad \boldsymbol{x}_B \ \geq \ \boldsymbol{0} \quad \text{and} \quad \boldsymbol{x}_N \ = \ \boldsymbol{0} \ . \tag{27}$$

Finally the gradient is calculated with

$$\boldsymbol{g}\left(\boldsymbol{\chi}\right) \ = \ \left(\frac{\partial \boldsymbol{c}_B}{\partial \boldsymbol{\chi}} - \boldsymbol{c}_B\boldsymbol{A}_B^{-1}\frac{\partial \boldsymbol{A}_B}{\partial \boldsymbol{\chi}}\right)\boldsymbol{x}_B \ . \tag{28}$$

Depending on the shape of the optimization function a step length α has to be given in order to scale the gradient steps. Moreover a sensitivity analysis is performed in the case of a break within the shape of the optimization function. Compared to the direct search method the gradient method yields the optimal solution very fast and in a straight manner though the robustness of the algorithm depends on the choice of an adequate step length. On the other hand the calculation effort of the direct search algorithm increases considerably with the number of branching points.

5.3 Yield-line prediction in context to the optimization strategies

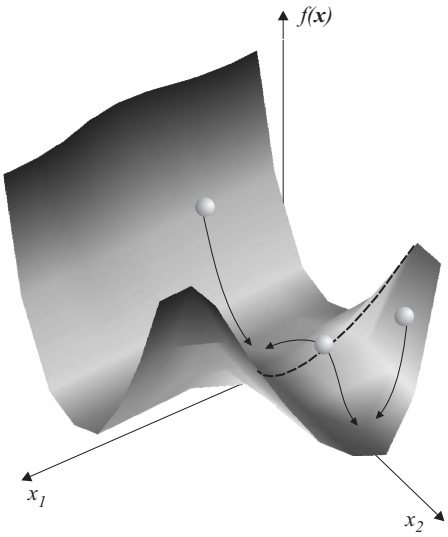

Figure 11: Shape of an optimization function

With regard to a typical topology of an optimization function as depicted in Fig. 11 it is important to choose an appropriate starting point in order to localize all possible minima. Depending on the condition of the problem there exist several local minima which sometimes admit to lead the search to another one. However, there is also the risk to get stuck in a wrong minimum without reaching the global one. In spite of that certain optimization procedures are able to find the right solution but in general the choice of the initial configuration decides about the course of the process.

Since the yield-line prediction algorithm gives a systematic estimate it can be assumed that all starting points are determined and in consequence all minima within the shape of the optimization function are detected.

6 Examples

The following examples illustrate the coaction between the algorithm for a yield-line prediction and the subsequent optimization procedure. In advance it can be noted that the calculation process as well as the localization of the global minimum of the ultimate load is improved decisively.

6.1 Example 1: Simply supported quadratic plate with a free edge

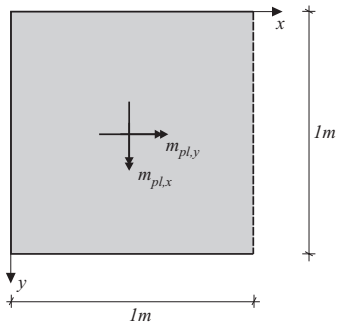

YLT $m_{pl,x} = m_{pl,y} = 1.00 \ \frac{kNm}{m}$
$m'_{pl,x} = m'_{pl,y} = 1.00 \ \frac{kNm}{m}$

FEM $h = 4.082 \ mm$
$f_{y,k} = 2.4 \cdot 10^5 \ \frac{kN}{m^2}$
J_2-plasticity, 20×20 mesh

Figure 12: Simply supported quadratic plate with a free edge

Firstly a simply supported quadratic plate with a free edge is considered with view on the yield-line prediction algorithm. The geometry and the plastic moments m_{pl} being the only necessary parameters for the yield-line theory (YLT) are shown in Fig. 12. There are $m_{pl,x}$ and $m_{pl,y}$ for the coordinate directions at the bottom of the plate and $m'_{pl,x}$ and $m'_{pl,y}$ at the top, respectively. The parameters of a finite element calculation (FEM) namely the plate thickness h and yield stress f_{yk}, using a nonlinear shell element based on J_2-plasticity, see [21], are given as well.

As three boundaries are simply supported and one is free the generation algorithm rotates three planes with an angle of 45^o and the fourth one with 90^o perpendicular to the reference plane of the considered plate like it is shown in Fig. 2. Thus the branching points are found, see Fig. 13a, while the degenerated fourth plane belonging to the free edge is to be eliminated.

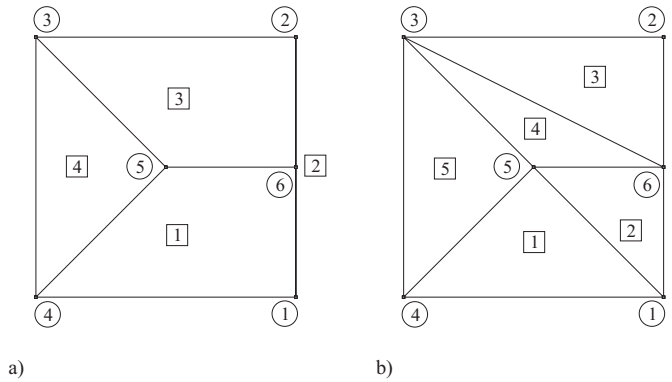

Figure 13: a) Yield-line prediction and b) Triangulation

The automatical triangulation yields a mesh which is depicted in Fig. 13b. The associated ultimate load is $p = 14.14 \frac{kN}{m^2}$. This corresponds very well to results of a geometrical non-linear finite element calculation, where an ultimate loading state could be defined at $p = 14.1 \frac{kN}{m^2}$. In this way the yield-line prediction algorithm delivers an adequate mesh being optimized by the presented optimization methods. Fig. 14 illustrates the yield zones determined by a finite element calculation together with the final yield-line pattern.

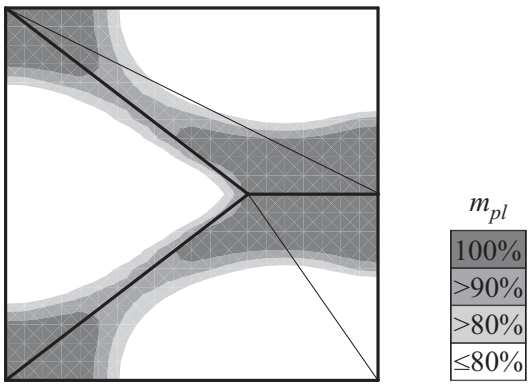

Figure 14: Yield zones and yield-line pattern after optimization process ($p = 14.14\frac{kN}{m^2}$)

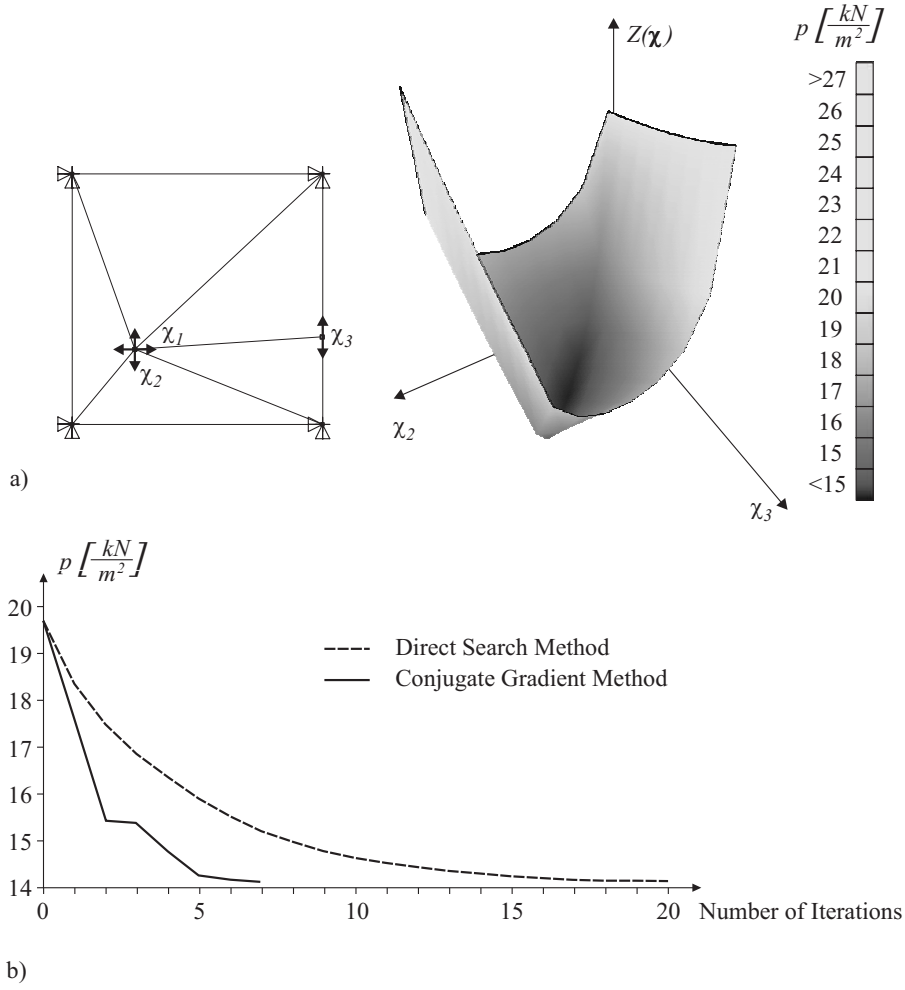

Figure 15: a) Degrees of freedom and optimization topology and b) convergence of optimization algorithms

Because of the realistic prediction symmetry conditions are mapped initially by active yield-lines. The connection between the nodes 3 and 6 exists only for triangulation and the calculation procedure proves that it will be inactive, as well as the line between the nodes 1 and 5. Furthermore the example shows that the use of a systematical yield-line prediction supports the optimization strategies in adjusting the coordinates of yield-line branching points.

In the present case the topology of the optimization function, depending on the searching degrees of freedom χ_2 and χ_3 (see Fig. 15a), is convex and very simple. In order to point out this property the triangulated mesh is now arbitrarily modified as it is shown in Fig. 15a. The direct search method and the conjugated gradient method lead both very fast to the minimum, see also [8]. However, Fig. 15b illustrates that the latter converges here much faster to the optimal solution, which could be observed often.

6.2 Example 2: Hexagonal plate with two different shapes

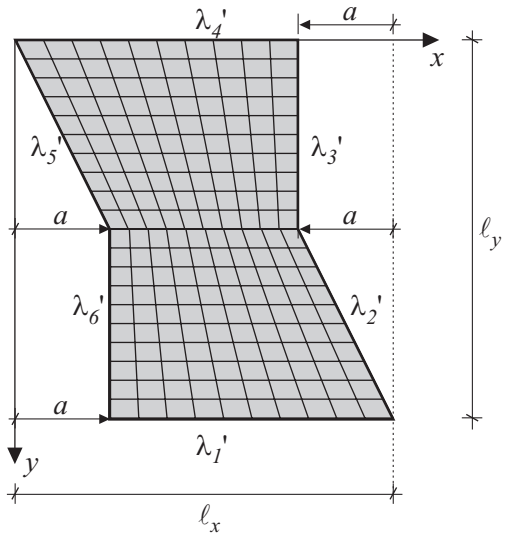

$$\ell_x = 1.00\ m$$
$$\ell_y = 1.00\ m$$
$$\lambda_i' = \frac{m_{pl,i}'}{m_{pl,x}} = 0$$

Version a): $a = -\frac{1}{4}\ell_x = -0.25\ m$

Version b): $a = +\frac{1}{4}\ell_x = +0.25\ m$

YLT	FEM
$m_{pl,x} = m_{pl,y} = 1.00\ \frac{kNm}{m}$	$h = 4.082\ mm$
$m'_{pl,x} = m'_{pl,y} = 0$	$f_{y,k} = 2.4 \cdot 10^5\ \frac{kN}{m^2}$
	J_2-plasticity, 20×20 mesh

Figure 16: Variation of the plate geometry

In order to study the influence of the shape of a structure, a variable hexagonal plate is considered, see Fig. 16. The parameter a will be varied. All edges are simply supported, determined by the quotient λ_i consisting of the belonging clamping moment $m'_{pl,i}$ referred to the plastic moment $m_{pl,x}$ of the plate's bottom. Moreover, the upper plastic moments $m'_{pl,x}$ and $m'_{pl,y}$ are zero, i.e. no negative moments can appear. The other variables are used accordingly to Example 1.

Before starting the optimization process the versions of $a = -\frac{1}{4}\ell_x$ and $a = +\frac{1}{4}\ell_x$ are distinguished with regard to the problem of a yield-line prediction. While the first version

leads to a unique yield-line pattern, see Fig. 17a, the presented algorithm yields the two yield-line patterns shown in Fig. 17b and c for the second version even though all directions of the rotation axes and the belonging rotation angles are exactly predetermined. In consequence it is proved evidently that the establishing of section 2.3 holds.

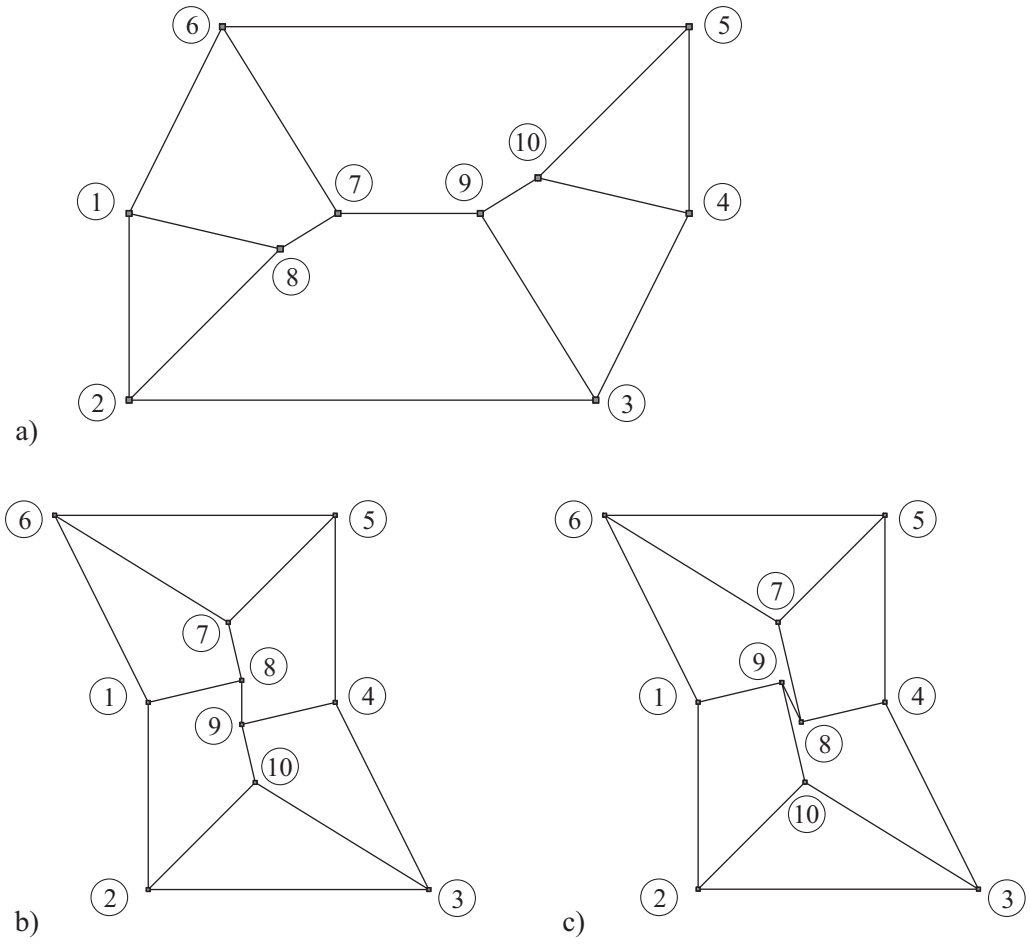

Figure 17: a) Yield-line pattern for Variation a, b) and c) Two admissible yield-line predictions for Variation b

The first version yields a load factor of $p = 17.43\frac{kN}{m^2}$ which is reduced to $p = 17.22\frac{kN}{m^2}$. As Fig. 18 shows, the yield zones of the finite element calculation encounter a similar result. However, the detected ultimate load is $p = 17.75\frac{kN}{m^2}$, being above the yield-line solution. Because the plate forms nearly an ellipsoidal boundary, the yield-line flexion is moderate in spite of the increasing area load. Thus the yield-lines develop relatively late and the comparison of the solutions of yield-line theory and finite element method has to be done in an earlier stage. In spite of that the two initial yield-line pattern predictions related to parameter $a = +\frac{1}{4}\ell_x$ lead to $p = 56.49\frac{kN}{m^2}$ and $p = 58.46\frac{kN}{m^2}$. With view to the intuitively simpler mode of Fig. 17b it is comprehensible that the first one yields the lower value. Whereas in the first version the development of yield zones was in the beginning, the finite element solution of the plate shows nearly entirely plastified regions in the second version. Thus the FEM–result $p = 54.40\frac{kN}{m^2}$ is lower than the value of $p = 56.06\frac{kN}{m^2}$ reached by an optimization process starting from the simpler configuration of the first version.

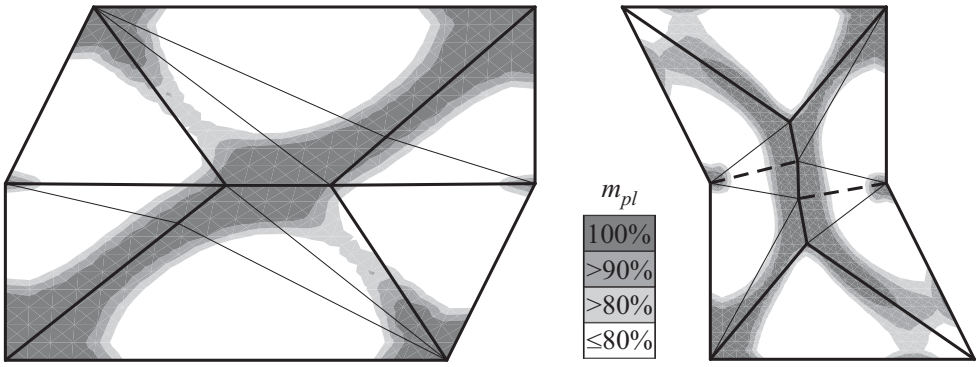

a) b)

Figure 18: Yield lines and zones for versions a): $p = 17.75\frac{kN}{m^2}$ and b): $p = 54.40\frac{kN}{m^2}$

Fig. 18 shows the yield-lines and the associated yield zones of the polygonal variations. Like other concavely shaped polygons the example shows considerably rotating yield-lines corresponding to sharply bordered yield zones. In this way the influence of a variation of the branching point coordinates react more sensitive than in the first case of a convex plate structure.

6.3 Example 3: Polygonal slab structure

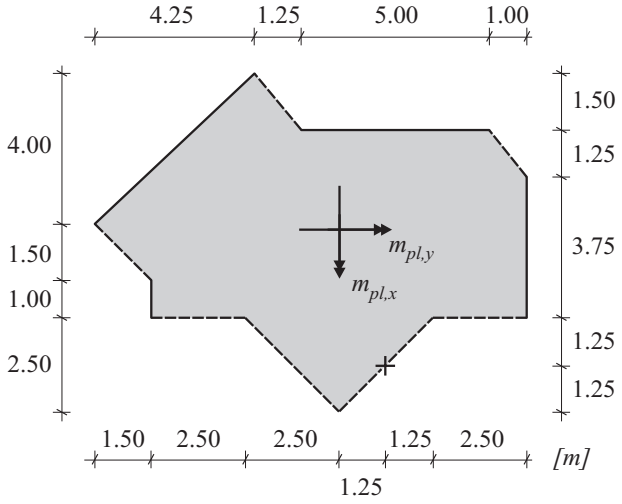

YLT	FEM
$m_{pl,x} = m_{pl,y} = 50\ \frac{kNm}{m}$	$h = 30.0\ cm$; $z = 0.67h$
$m'_{pl,x} = m'_{pl,y} = 50\ \frac{kNm}{m}$	$f_{y,k} = 5.0 \cdot 10^5\ \frac{kN}{m^2}$
	$a_{sl} = 5.0\ \frac{cm^2}{m}$; $a_{su} = 5.0\ \frac{cm^2}{m}$

Figure 19: Polygonal slab structure

In the papers [4], [11] and [10] a polygonal slab was presented which shall be considered

now with the proposed algorithm. Due to the lack of description in literature the geometric parameters are assumed as shown in Fig. 6.3. The parameters of the yield-line theory (YLT) are given as usual. Since the plate is modelled as a isotropic concrete structure the internal lever arm z is defined as two third of the thickness h whereas the upper reinforcement a_{su} is chosen equal to the lower reinforcement a_{sl}. In the finite element calculation (FEM) the yield stress parameter $f_{y,k}$ of steel is assumed.

Using the presented yield-line prediction algorithm, two admissible yield-line configurations are found by rotating the several planes, see Fig. 20. The subsequent triangulation procedure yields the results shown in Fig. 21. However, it can be stated that differences are only found on the left hand side of the plate.

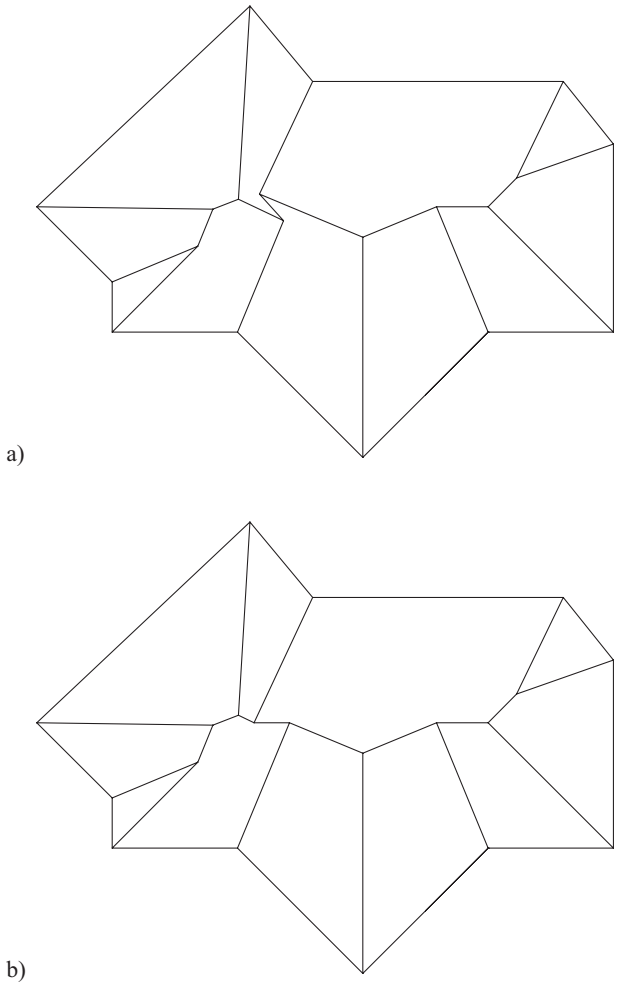

Figure 20: Two admissible yield-line predictions for a polygonal slab structure

In view of the considerable number of branching points and in consequence also of the degrees of freedom being subject to the optimization algorithm it is more advisable to perform the conjugate gradient method.

Thus the first mechanism leads to an initial load level of $p = 19.48\frac{kN}{m^2}$, the second one to $p = 19.24\frac{kN}{m^2}$. This gap can be explained with the two nearly identical configurations. Furthermore the obviously simpler mechanism is the lower one.

At the end of the optimization procedure which causes another reduction to $p = 17.39\frac{kN}{m^2}$

and $p = 17.15\frac{kN}{m^2}$ respectively, the triangulation patterns of Fig. 22 are reached. The shaded areas mark the yield zones detected by the nonlinear finite element calculation.

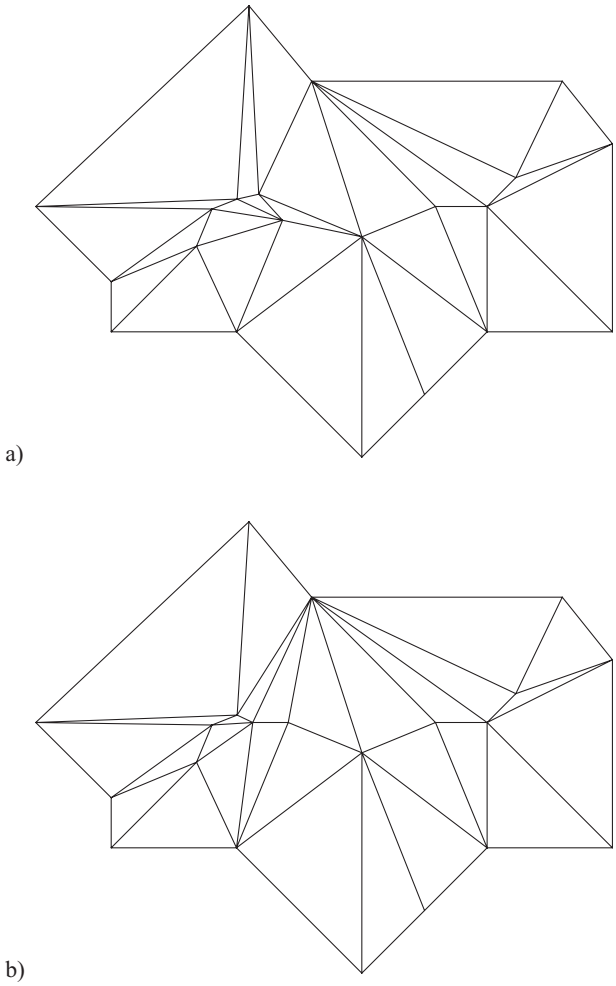

Figure 21: Triangulation of the yield-line predictions

It can also be seen that the deformation behaviour of the constantly loaded plate is given correctly. The comparison to the finite element solution confirms a good accordance between the mechanisms whereas a certain difference within the lower left half of the plate results by the flat deflection in the corresponding area. Thus the deviation is compensated by little yield-line angles. Finally, the determined ultimate load is $p = 16.2\frac{kN}{m^2}$, which is about 5% to 7% lower than the detected limit load. This is a considerably good result compared to the complexity of the plate.

In this example the two different yield-line predictions lead to a nearly identical result due to their close relationship. However, it must be stated that multiple independent solutions may exist, especially with regard to an increasing complexity. Even if specialized optimization approaches help to overcome discontinuities between the belonging optimization topologies this example emphasizes the necessity of a systematical and objective initial yield-line prediction.

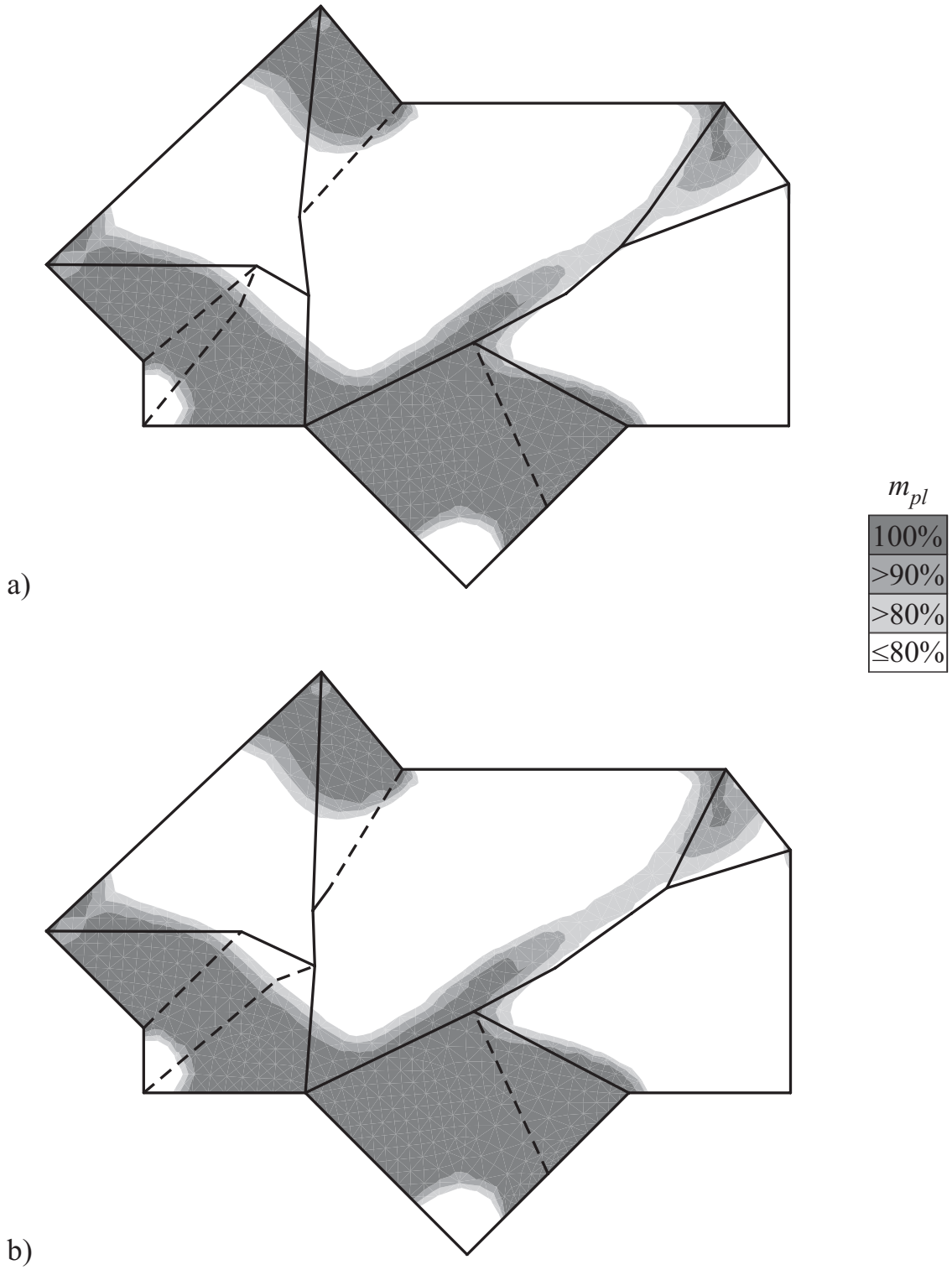

Figure 22: Yield zones and final yield-line patterns of both predictions ($p = 17.39\frac{kN}{m^2}$ and $p = 17.15\frac{kN}{m^2}$)

7 Conclusions

The presented yield-line prediction algorithm is the completion to the triangular yield-line element approaches introduced by [1] and [15]. Using a new application of the Catalan numbers it determines all admissible yield-line patterns and thus it gives the possibility to check all the related kinematical mechanisms systematically. As it has been shown in the examples, the simple definition of the direction and also the angles of rotation axes are not sufficient to determine yield-line patterns unequivocal. Furthermore, all conceivable yield-lines and in consequence the belonging yield-line configurations are detected and represented into a subsequent optimization procedure. In this way all areas within the optimization function are detected in order to be performed by a searching process.

Several examples illustrate the possibility of multiple solutions of initial yield-line patterns. It can be shown that the application of optimization procedures lead to satisfying results of the ultimate load of plate structures using the yield-line theory. Thus the yield-line theory provides a considerable tool to predict limit loads beside nonlinear finite element calculations. The concentration of the plastic regions in yield lines leads to a clear understanding of the load bearing behavior in a design process.

References

[1] Anderheggen, E. / Knöpfel, H.: *Finite element limit analysis using linear programming.* International Journal of Solids and Structures 8 (1972), p. 1413–1431.

[2] Bege, A. / Kása, Z.: *Coding Objects Related to Catalan Numbers.* Studia Univ. Babeş-Bolyai, Informatica XLVI (2001), p. 31–40.

[3] Beineke, L. W. / Pippert, R. E.: *A census of ball and disk dissections.* Lecture Notes in Mathematics 303 (1972), p. 25–40.

[4] Damkilde, L. / Krenk, S.: *Limits – A system for limit state analysis and optimal material layout.* Computers & Structures 64 (1997), p. 709–718.

[5] Fletcher, R. / Reeves, C. M.: *Function minimization by conjugate gradients.* The Computer Journal 7 (1964), p. 149–154.

[6] Hooke, R. / Jeeves, T. A.: *"Direct search" solution of numerical and statistical problems.* Journal of the Association for Computing Machinery 8 (1961), p. 212–229.

[7] Jennings, A.: *On the identification of yield-line collapse mechanisms.* Engineering Structures 18 (1996), p. 332–337.

[8] Jennings, A. / Thavalingam, A. / McKeown, J. J. / Sloan, D.: *On the Optimisation of Yield Line Patterns.* Developments in Computations Engineering (1993), p. 209–213.

[9] Johansen, K. W.: *Brudlinieteorier.* Jul. Gjellerups Forlag, København, 1943.

[10] Krabbenhoft, K. / Damkilde, L.: *Lower bound limit analysis of slabs with nonlinear yield criteria.* Computers & Structures 80 (2000), p. 2043–2057.

[11] Krenk, S. / Damkilde, L. / Høyer, O.: *Limit analysis and optimal design of plates with equilibrium elements.* Journal of Engineering Mechanics 120 (1994), p. 1237–1255.

[12] Kwan, A. K. H.: *Dip and strike angles method for yield line analysis of reinforced concrete slabs.* Magazine of Concrete Research 56 (2004), p. 487–498.

[13] McKeown, J. J. / Jennings, A. / Thavalingam, A. / Sloan, D.: *Optimization Techniques for Generating Yield-Line Patterns.* Advances in Structural Optimization (1994), p. 161–169.

[14] Munro, J.: *The elastic and limit analysis of planar skeletal structures.* Civil Engineers & PWR 60 (1965), p. 674–677.

[15] Munro, J. / DaFonseca, A. M. A.: *Yield line method by finite elements and linear programming.* The Structural Engineer 56B (1978), p. 37–44.

[16] Munro, J. / Smith, D. L.: *Linear programming in plastic analysis and synthesis.* Proceedings International Symposium Computer-Aided Structural Design, University of Warwick 1 (1972), p. A1/22–A1/54.

[17] Ramsay, A. / Johnson, D.: *Geometric optimization of yield–line patterns using a direct search method.* Structural Optimization 14 (1997), p. 108–115.

[18] Siemon, H.: *Anwendungen der elementaren Gruppentheorie in Zahlentheorie und Kombinatorik.* S. 40–47, Klett, 1981.

[19] Thavalingam, A. / Jennings, A. / McKeown, J. J. / Sloan, D.: *A computerised method for rigid-plastic yield-line analysis of slabs.* Computers & Structures 68 (1998), p. 601–612.

[20] Wüst, J.: *Formfindung der Fließliniengeometrie für polygonale Platten im Traglastzustand.* Dissertation (2006), Institut für Baustatik, Universität Karlsruhe.

[21] Wagner, W. / Gruttmann, F.: *A robust nonlinear mixed hybrid quadrilateral shell element.* International Journal for Numerical Methods in Engineering 64 (2005), p. 635–666.